Computational Challenges in High Angle of Attack flow

Muhammad Amjad Sohail[1], Prof. Yan Chao[2], Rizwan ullah[3], Muhammad Yamin younis[4]

***Abstract*—**Side force occurrence on slender bodies of revolution at high angle-of-attack ($AOA > 30^o$) has long been observed by experimenters. Flow-field features for a slender body at high *AOA* recently have received considerable attention in the recent year's .These studies demonstrate that flow separating from the body rolls up into a pair of asymmetric vortices between $30^o < AOA < 70^o$.Significant side force results from asymmetric vortices. The magnitude of this side force can equal that of the normal force acting on the slender body, which causes an aircraft to spin or a missile to tumble in situations where these effects are not thoroughly considered as part of the control system design. It is also found that side force distribution exhibited an oscillatory behavior along slender body. In this study, CFD simulations are performed to calculate side force on high angle of attack without any side angle. It is found that this asymmetrical pair of vortices strengths increases as we move backward from the tip and if slenderness ratios is increased then exhibited side force is also increased. The CFD algorithm directly cannot calculate or simulate the side force without side angle because it is symmetric in nature. So in this research study methods are suggested how to calculate the side force with zero side angle. So in this research study computational challenges at high angle of attack are studied and simulated.

***Keywords*—**Detached eddy simulation, dual time stepping, hypersonic flow, turbulence modeling

I. Introduction

THE Side force occurrence on slender bodies of revolution at high angle-of-attack ($AOA > 30^o$) has long been observed by experimenters. Flow-field features for a slender body at high *AOA* recently have received considerable attention.1−6.These studies demonstrate that flow separating from the body rolls up into a pair of asymmetric vortices between $30^o < AOA < 70^o$.Significant side force results from asymmetric vortices. The magnitude of this side force can equal that of the normal force acting on the slender body, which causes an aircraft to spin or a missile to tumble in situations where these effects are not thoroughly considered as part of the control system design. Zilliac *et al*.2 reported even as small as dust particles (~ 3 μm) incidentally coating the nose of the model, were found to change direction and phase of side force distribution. The finding implies that leading-edge vortex genesis and subsequent growth are highly sensitive to small imperfections of the nose tip. Lamont *et al*.3 found that side force distribution exhibited an oscillatory behavior along slender body. In this study, CFD simulations are performed to calculate side force on high angle of attack without any side angle and slenderness effect on side force is investigated.[7] says a variety of difficulties arise when performing high angle of attack computations, including challenges in properly modeling turbulence and transition for vortical and massively separated flows, the need to use appropriate numerical algorithms if flow asymmetry is possible, and the difficulties in creating grids that allow for accurate simulation of the flowfield. These issues are addressed and recommendations are made for further improvements in high angle of attack flow prediction. When angle of attack is increased then flow behavior is changed these all phenomena are depicted in figure (1) and (2) and detail of the same in given in references [8-11]. In ref [12], Degani D, Levy Y. studies the experimentally asymmetric turbulent vortical flows over slender bodies. Ref [13] demonstrates the forces and moments collected in the analysis revealed a sharp change in the side force at extremely high angles of attack. Although the position and shape of the spike varied with Reynolds number and boundary-layer state, the change was always apparent. The single strake case demonstrated that the clean and tripped side force change was not insignificant. The dual strake case demonstrated that the phenomena could be controlled by controlling the separation on the side of the forebody. MARCUS S. W.[14] says that objections have been raised regarding the justification for utilizing the thin-layer Navier-Stokes (TLNS) model to study flow asymmetries, because the viscosity effect of the circumferential and streamwise flow components might become important at the high attack angles of interest. The CFD algorithm directly cannot calculate or simulate the side force without side angle because it is symmetric in nature. So in this research study methods are suggested how to calculate the side force with zero side angle. For these calculations SA turbulent model and DES approach is used [15-21]. The current authors used the same SA model and DES (Detached Eddy simulation) for supersonic and hypersonic flows by using SA model and DES techniques. Different Authors used unstructured finite-volume solver *Cobalt* in conjunction with DES successfully on a number of complex problems, including a supersonic base flow[22], delta wing vortex breakdown[23], a square with rounded corners[24][23], the F-15E at high angle of attack[25], and the F/A-18E with unsteady shock buffet[26][25].

DES is a three-dimensional, time-dependent approach which properly resolves the above mentioned phenomena by using hybrid philosophy of RANS and LES approaches on the expense of little increase in cost. The present study deals with

Muhammad Amjad Sohail is PhD student from Beijing University of Aeronautics and Astronautics Beijing China (phone: 0086-13120491221; e-mail: masohailamer@ yahoo.com).

Prof. Yan Chao is professor from Beijing University of Aeronautics and Astronautics Beijing China (phone: 0086-13501200881; e-mail: chyan@vip.sina.com@ yahoo.com).

Muhammad Yamin Younis is PhD student from Beijing University of Aeronautics and Astronautics Beijing China (phone: 0086-13120491221; e-mail: mrmukkarum@yahoo.com).

the detail implementation of time dependent DES approach and RANS approaches. First the RANS approach using Sparllart Almaras turbulent model is used and the aerodynamics characteristics are calculated for cone-cylinder and frustrum configurations. Then time dependent DES approached is used by using implicit solver and implicit time stepping (dual time steeping formulation) is used to simulate the subsonic flow at low Mach number. The second order Euler backward time stepping is used for the same. The finite volume and multiblock implicit solver is used for these calculations. Finally the simulated results are compared with the available experimental as well as theoretical.

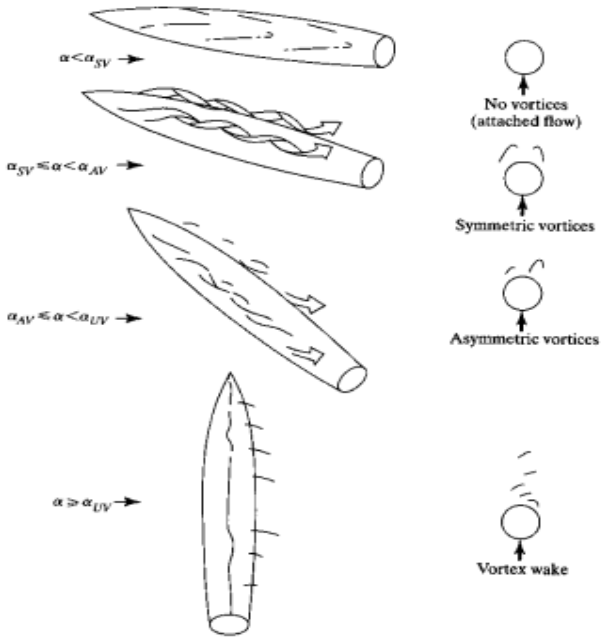

Fig: 1 Angle of attack flow regimes (aSV is the angle of attack where symmetric vortices are formed, aAV is the angle of attack where asymmetric vortices are formed, and aUV is the angle of attack where an unsteady vortex wake is formed; from [1–4])

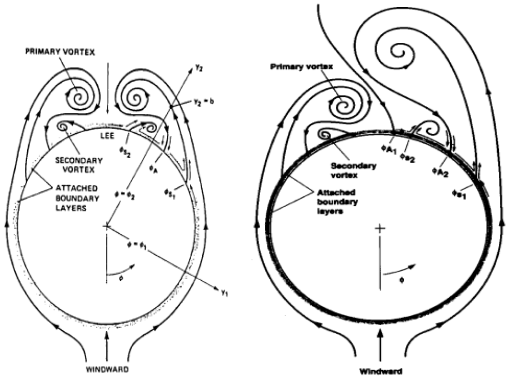

Fig: 2 Slender body flow topology at medium and high angles of attack

In the above it is explained when angle of attack is increased from medium to high then the asymmetrical vortices are being generated. At very high angle of attack the vortex wake is generated. So for capturing these phenomena, CFD algorithm is modified. SA model and Detached eddies simulations techniques are used. The flow is subsonic (35km/hr) so preconditioning is used here to give some numerical stiffness to the solution [47].

II. Geometrical Models

In the present investigation, Three different models have been used, namely (a) blunt cone with after body (b) blunt cone with after body and 5° frustum and (c) blunt cone with after body with 10° frustum, as shown in Fig.1 The first test model (blunt cone with after body) has been chosen for its simple design and represents AGARD configuration, HB-1 (Hypervelocity Ballistic model). The first part of the model is a blunt cone which has an apex angle of 41◦ and length of 40.6mm. The second part of the model is the cylinder of 51mm outer diameter and a length of 186mm. The model has a spherical nose radius of 15mm. The second and third test model (Blunt cone with after body and frustum) represents a simple AGARD configuration, HB-2. The geometry of the blunt cone remains the same and the length of the cylinder is reduced to 111mm with the outer diameter of 51mm. The frustum has an axial length of 75mm with a semi-vertex angle of 5◦ and 10°. For these three configurations, the total length of the model has been kept the same in order to maintain the exact L/D (i.e., length to diameter) ratio of the model. The details and test conditions are mentioned in reference [36]

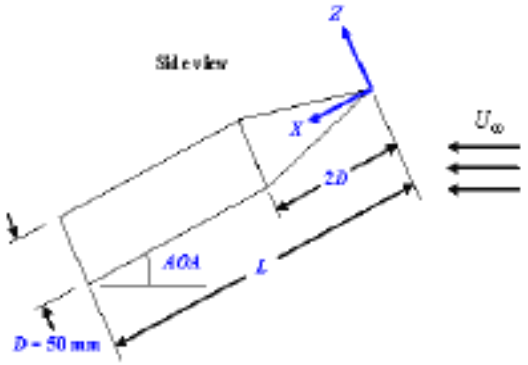

Fig: 3 Geometrical Model

III. Mesh Generation and Wall Roughness

The algebraic method is used to generate three-dimensional boundary-fitted grids for blunt cone configurations. The height of the first grid next to the body is controlled, and the grids near to the body are normalized to achieve y+ less than 1. The H-H and C-type boundary- fitted grids are generated at first in order to simulate the aerodynamic forces accurately. The mesh for Detached Eddy simulation is created very carefully. In shock wave region and corner expansion and compression regions and wake regions is meshed with very high accuracy so that the expansion ratio should be remained below 1.2. Detailed study of Mesh generations for detached eddy simulations is given in reference [37]. Three different types of study are performed to calculate the side force.

A. Flow condition and asymmetric disturbance

The flow condition of Mach number, 0.12 is chosen in the numerical simulation owing to the availability of the experimental data. The angles of attack with a range of 20-70 degrees are considered. The experiment indicates the asymmetric vortices structure at the angle of attack above 30 degrees, while the computation shows the symmetric structure, owing to the symmetric nature of the present numerical algorithm.

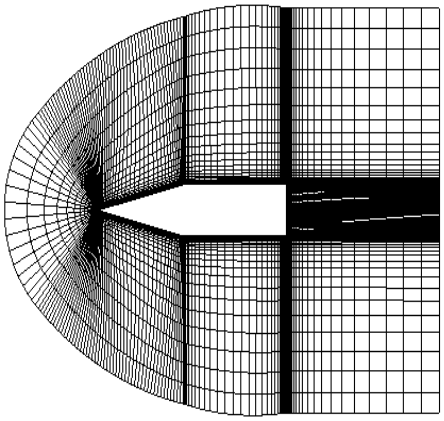

Fig. 4(a) Generation of mesh

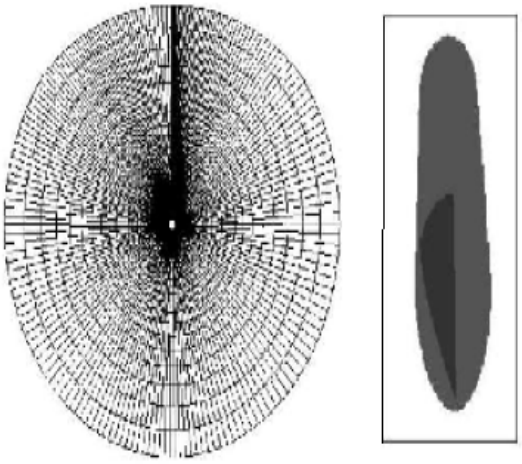

Fig. 4(b) Asymmetrically clustered grid system and location of asymmetric roughness in the forward part of the slender body

This finding implies that some types of artificial asymmetric disturbance are necessary to simulate the asymmetric structure arising in physical flow by the numerical method. In this study, three types of asymmetric disturbances are tested; grid, sideslip angle, and wall roughness. At first, the grid system for generating an asymmetry vortex shows at the left side in the figure 4. It means asymmetrically clustered grids of left and right side is assumed that there is a possibility to generate the different vortex pattern based on numerical errors due to the difference of grids. Then side slip angle is applied only 1 degree. It is an easy way to touch and apply for a numerical analysis. Finally, a special roughness area is applied. In the case of wall roughness, previous studies show that the mean velocity distribution near rough walls has a different intercept, in other words, an additive constant in the log-law [48].

IV. Governing Equations and Turbulence Models

A. Governing Equations

The system of governing equations for a single-component fluid, written to describe the mean flow properties, is cast in integral Cartesian form for an arbitrary control volume V with differential surface area dA as follows:

$$\frac{\partial}{\partial t}\int_V W dV + \oint [F - G].dA = \int_V H dV \tag{1}$$

Where the vectors W, F and G are defined as:

$$W = \begin{bmatrix} \rho \\ \rho u \\ \rho v \\ \rho w \\ \rho E \end{bmatrix}, F = \begin{bmatrix} \rho u \\ \rho vu + P\hat{i} \\ \rho vv + P\hat{j} \\ \rho vw + P\hat{k} \\ \rho vE + Pv \end{bmatrix}, G = \begin{Bmatrix} 0 \\ \tau_{xi} \\ \tau_{yi} \\ \tau_{Zi} \\ \tau_{ij} v_j + q \end{Bmatrix}$$

Vector H contains source terms such as body forces and energy sources.

Here ρ, v, E, and p are the density, velocity, total energy per unit mass, and pressure of the fluid, respectively. T is the viscous stress tensor, and q is the heat flux.

Total energy E is related to the total enthalpy H by

$$E = H - p/\rho \tag{2}$$

Where $H = h + \frac{|v|^2}{2}$

B. Turbulence Model

To calculate the turbulent flows the SA turbulent model [21] is used here. The transported variable in the Spalart-Allmaras model, $\tilde{\nu}$, is identical to the turbulent kinematic viscosity except in the near-wall (viscous-affected) region. The transport equation for $\tilde{\nu}$ is

$$\frac{\partial}{\partial t}(\rho\tilde{\nu}) + \frac{\partial}{\partial x_i}(\rho\tilde{\nu}u_i) = G_\nu + \frac{1}{\sigma_{\tilde{\nu}}}\left[\frac{\partial}{\partial x_i}\left\{(\mu + \rho\tilde{\nu})\frac{\partial\tilde{\nu}}{\partial x_j}\right\} + C_{b2\rho}\left(\frac{\partial\tilde{\nu}}{\partial x_j}\right)^2\right] - Y_\nu + S_{\tilde{\nu}} \tag{3}$$

Where G_ν is the production of turbulent viscosity and Y_ν is the destruction of turbulent viscosity that occurs in the near-wall region due to wall blocking and viscous damping. $\sigma_{\tilde{\nu}}$ and

C_{b2} are constants and ν is the molecular kinematic viscosity. $S_{\tilde{\nu}}$ is a user-defined source term.

C. DES Model

In the DES approach [17,40-46], the unsteady RANS models are employed in the near-wall regions, while the filtered versions of the same models are used in the regions away from the near-wall. The LES region is normally associated with the core turbulent region where large turbulence scales play a dominant role. In this region, the DES models recover the respective subgrid models. In the near-wall region, the respective RANS models are recovered so we can say DES is the hybrid model of LES and RANS. The standard Spalart-Allmaras model uses the distance to the closest wall as the definition for the length scale d, which plays a major role in determining the level of production and destruction of turbulent viscosity as given respectively.

$$\tilde{S} = S + \frac{\tilde{\nu}}{k^2 d^2} f_{v2} \qquad (4)$$

$$Y_v = C_w \rho f_w \left(\frac{\tilde{\nu}}{d}\right)^2 \qquad (5)$$

$$r = \frac{\tilde{\nu}}{\tilde{S} k^2 d^2} \qquad (6)$$

The DES model, as proposed by Shur et al. [9] replaces d everywhere with a new length scale $\tilde{d}$, defined as

$$\tilde{d} = \min\left(d, C_{des}, \Delta\right) \qquad (7)$$

Where the grid spacing, Δ, is based on the largest grid space in the x, y, or z directions forming the computational cell. The empirical constant C_{des} has a value of 0.65.

D. DES Model

The implicit-time stepping method (also known as dual-time formulation) is used here for the calculation of detached eddy simulation in the implicit formulation. Density based implicit solver is used for both RANS and LES simulations with SA and K-ω SST turbulence modeling. Preconditioned pseudo-time-derivative term is used here

$$\frac{\partial}{\partial t}\int_V W dV + \Gamma \frac{\partial}{\partial \tau}\int_V Q dV + \oint [F - G].dA = \int_V H dV \qquad (8)$$

Where t denotes physical-time and τ is a pseudo-time used in the time-marching procedure. If as $\tau \to \infty$, the second term on the left side of Equation (4) vanishes. The time-dependent term in Equation (4) is discretized in an implicit fashion by means of either a first- or second-order accurate, backward difference in time. The dual-time formulation is written in semi-discrete form as follows which is second order accurate for these simulations:

$$\left[\frac{\Gamma}{\Delta\tau} + \frac{\varepsilon_0 \partial W}{\Delta t \partial Q}\right]\Delta Q^{K+1} + \frac{1}{V}\oint [F - G].dA = H - \frac{1}{\Delta t}\left(\varepsilon_0 W^k - \varepsilon_1 W^n + \varepsilon_2 W^{n-1}\right) \qquad (9)$$

Physical time step Δt is limited only by the level of desired temporal accuracy. The pseudo-time-step $\Delta\tau$ is determined by the CFL condition of the time-marching scheme. Normally physical time step is taken as 0.00001 to 0.001s and 500 time steps are taken for these computations. The convective fluxes are calculated by using AUSM+ and all other equations like turbulence etc are taken as second order accurate.

V. Results and Discussion

The test conditions for these simulations are M_∞ is taken as 0.12 P_∞ 101325 pa and T_∞ is 300°k and the convergence criteria for these simulations is taken as for continuity and energy equations is 10^{-4} and for x,y,z velocities and others quantities 10^{-5} to 10^{-6}. For turbulent model the steady state simulations are performed but for DES computations unsteady time dependent dual time stepping implicit solver is used. First model cone-cylinder is simulated at Mach number 8 with sparllart almaras turbulent model and DES with SA model and angle of attack 0° to 70°. The simulated results for angle of attack 60° are shown in figure (5). Contours of Mach number, dynamics pressure, pressure, turbulence viscosity, total energy, vorticity magnitude are shown for DES computations. These all contours show that asymmetrical phenomenon can be seen at high angle of attack. Asymmetrical pairs of vortices normally clearly visible in the contours of Mach number, vorticity and pressure. The best method to capture this phenomenon is to create a portion of wall roughness which exhibits this phenomenon by creating numerical disturbances on the left and right side of leeward and windward side. In figure (6) and (7) different contours at angle of attack 50° and 70° are shown and showing the same phenomena.

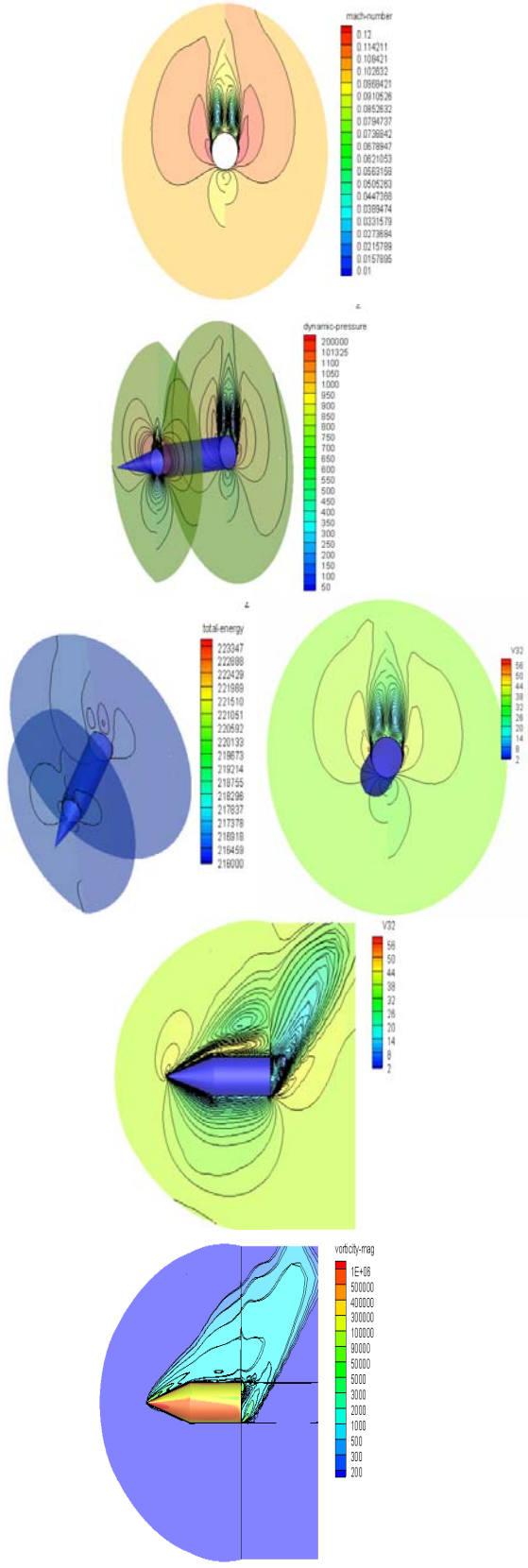

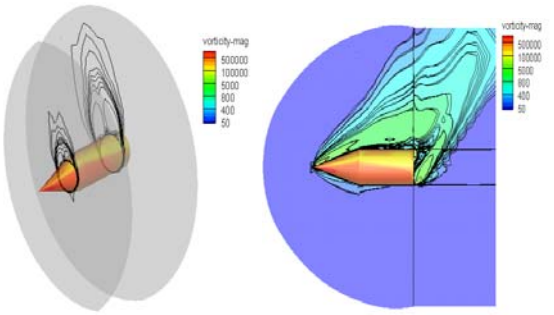

Fig. 5 contours of Mach number dynamic pressure, pressure and other quantities for cone-cylinder at angle of attack 60^{o} and Mach number for DES computations

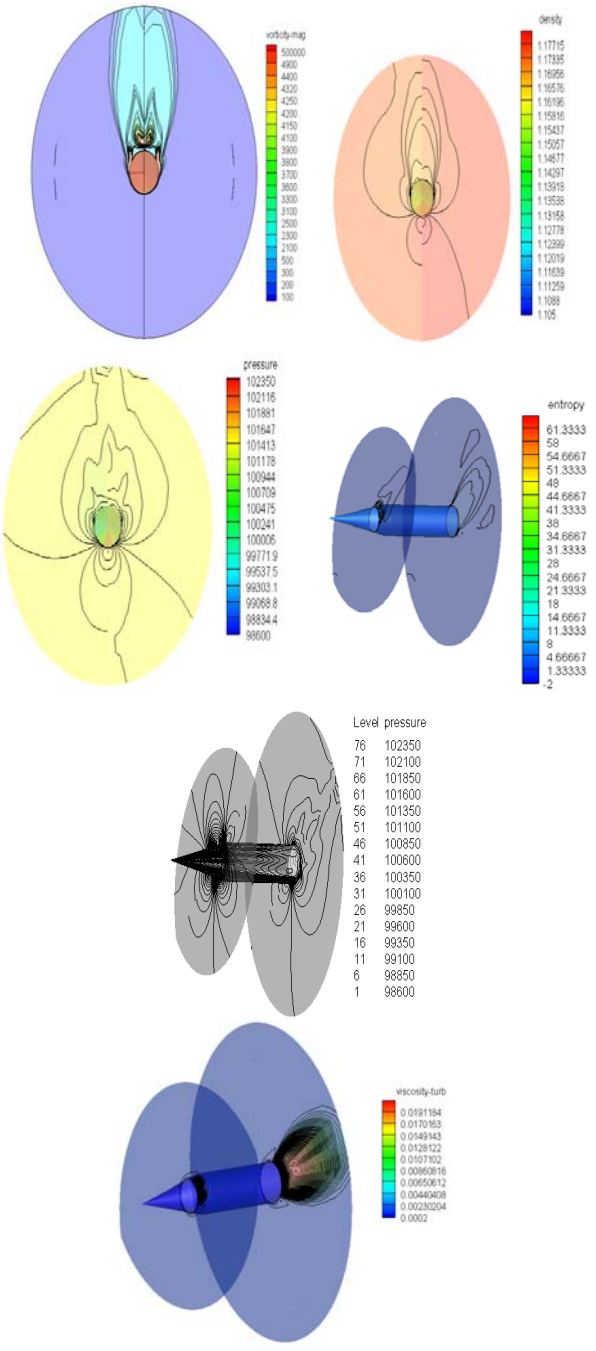

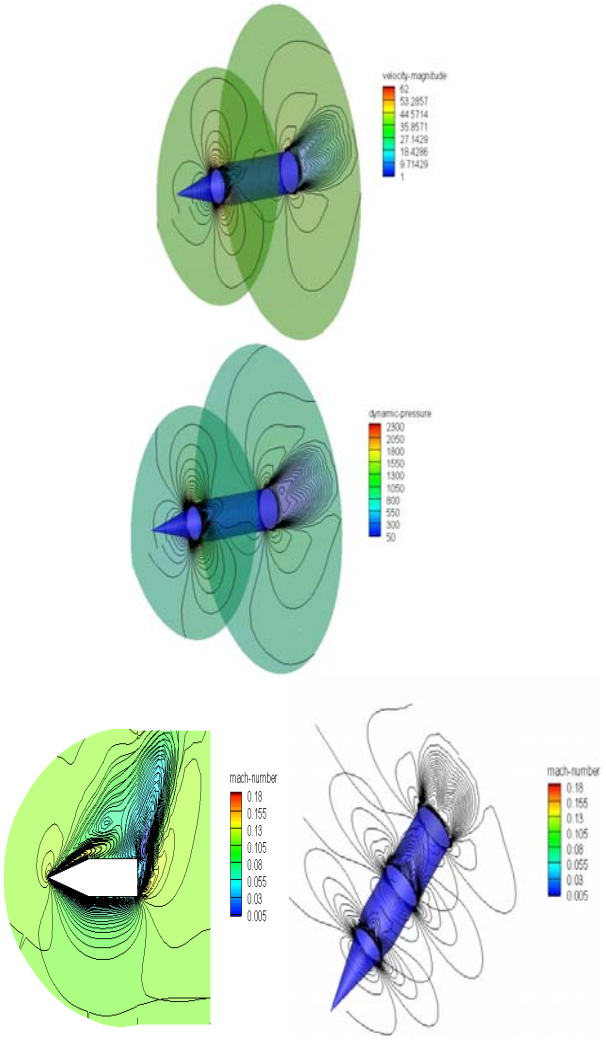

Fig. 6 contours of Mach number number dynamic pressure, pressure and other quantities for cone-cylinder at angle of attack 70^{o} for DES computations

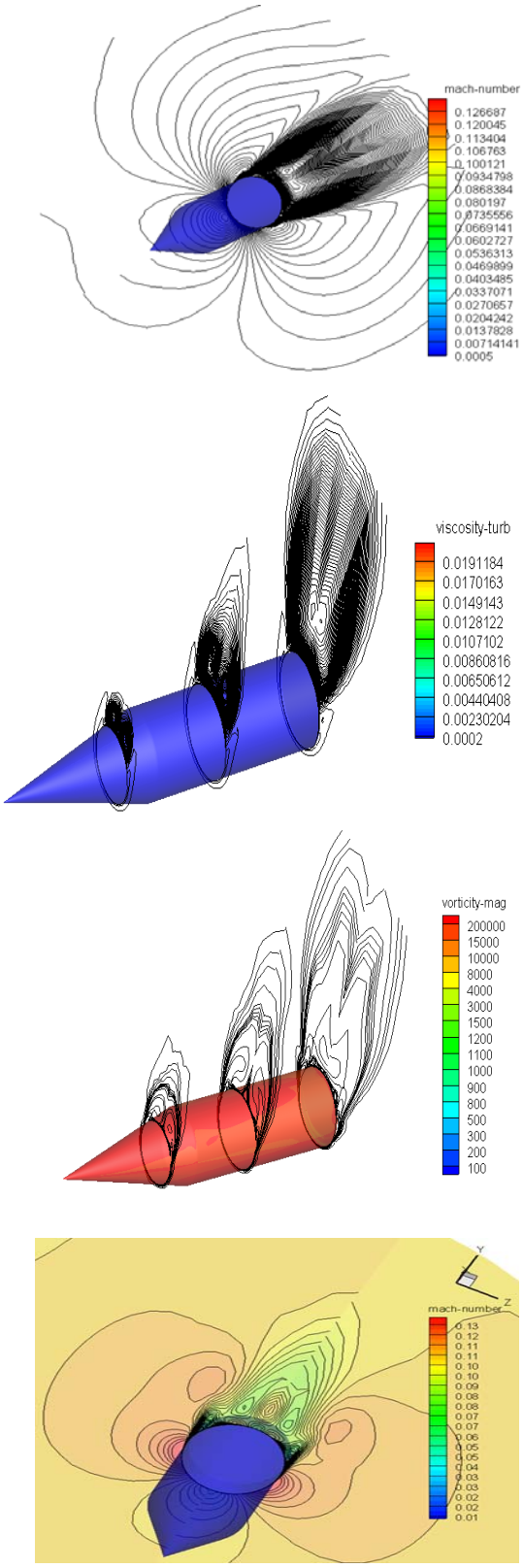

Fig. 7 contours of Mach number density, total pressure and temperature for cone-cylinder at angle of attack 50^{o} and Mach number for DES computations

In figure (8) side force on cone cylinder body is compared with experimental results. From angle of attack 0^o to 30^o side force is observed very less. But when angle of attack is increased from 35^o to 50^o the side force is increased and then side force beyond 50^o angle of attack is decreased.

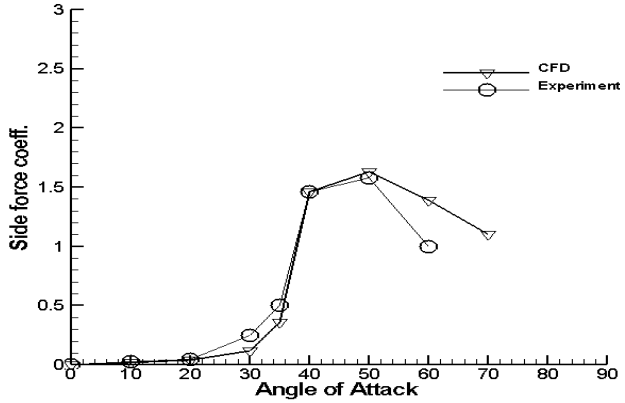

Fig. 8 Side force vs angle of attack for DES

VI. Conclusion

DES simulations are performed at low Mach number and high angle of attacks by using SA model, DES and dual time stepping implicit formulations. The computed results are compared with experimental data. The CFD algorithm is symmetrical so it is modified to accommodate the disturbance to calculate the side force due to unsymmetrical vortices. The numerical disturbance is created by using variable mesh density on the upper side or leeward side, little side slip angle or using the wall roughness parameter. The computed results show that by using the above mentioned techniques the unsymmetrical phenomena are captured. Two distinct pairs of vortices on the leeward side are observed which the cause the asymmetry is as well as side force. Turbulent model SA and DES resolved the boundary layers and high pressure gradient flows and shows acceptable results in boundary layers and wake expansion compression and separated region with y+ value less than 1. But when the same configurations are simulated with DES model then the wall regions and wake regions are properly resolved the turbulent viscosity is properly resolved by DES model by using the RANS and LES version of the same. The mesh is little modified for the LES part of the DES model to properly resolve the turbulent viscosity where the turbulent length scales is increased. So from these computations we have concluded that with the little expense of cost the DES models gives the better results for highly turbulent flows by using the RANS and LES nature of the model. The side force results at high angle of attack are calculated and it has excellent agreement with available data.

References

[1] K. D. Thomson and D. F. Morrison, *Journal of Fluid Mechanics* **50**, Part 4 (1971) 751−783.

[2] G. G. Zilliac, D. Degani and M. Tobak, *AIAA Journal* **29**(5) (1991) 667−675.

[3] . J. Lamont and B. L. Hunt, *Journal of Fluid Mechanics* **76**, Part 3 (1976) 519−559.

[4] D. Degani and Y. Levy, *AIAA Journal* **30**(9) (1992) 2267−2273

[5] . E. Ericsson, *Progress in Aerospace Sciences* **31** (1995) 291−334

[6] P. Liu and X. Deng, *Canadian Aeronautics and Space Journal* **49**(1) (2003) 31−40

[7] Russell M. Cummings [a], James R. Forsythe [b], Scott A. Morton [b], Kyle D. Squires" Computational challenges in high angle of attack flow prediction" *Aerospace Engineering Department, California Polytechnic State University, San Luis Obispo, CA 93407, USA*

[8] Keener ER, Chapman GT. Similarity in vortex asymmetries over slender bodies and wings. AIAA J 1977;15: 1370–2

[9] Rom J. High angle of attack aerodynamics. New York: Springer, 1992

[10] Ericsson LE, Reding JP. Asymmetric vortex shedding from bodies of revolution. In: Hemsch MJ, Nielsen JN, editors. Tactical missile aerodynamics. New York: American Institute of Aeronautics and Astronautics, 1986.

[11] Bertin JJ. Aerodynamics for engineers. Upper Saddle River, NJ: Prentice-Hall, 2002.

[12] Degani D, Levy Y. Asymmetric turbulent vortical flows over slender bodies. AIAA J 1992;30(9):2267–73

[13] Jason M. Merret* and Michael B. Bragg" X-38 AERODYNAMICS DURING RAPID PITCH UP" University of Illinois at Urbana-Champaign Urbana, IL 61801AIAA 2003-3526

[14] Degani D, Marcus SW. Thin vs. full Navier–Stokes computation for high-angle-of-attack aerodynamics. AIAA J 1997;35(3):565–7

[15] F. Lesage, J. Nicolle, and M. A. Boulianne, *Navier-Stokes computations of high angle of attack missile flowfields,* AIAA paper 2000-4212, (2000)

[16] Spalart PR, Jou W-H, Strelets M, Allmaras SR. Comments on the feasibility of LES for wings, and on a hybrid RANS/LES approach. Advances in DNS/LES, First AFOSR International Conference on DNS/LES, Rusliton, CA, Greyden Press, Columbus, 1997

[17] Shur M, Spalart PR, Strelets, M, Travin A. Detached-eddy simulation of an airfoil at high angle of attack. Proceedings of the Fourth International Symposium on Engineering Turbulence Modeling and Measurements. Amsterdam: Elsevier Science, 1999. p. 669–78

[18] B. CARUELLEa, and F. DUCROSb" Detached-Eddy Simulations of Attached and Detached Boundary Layers" International Journal of Computational Fluid Dynamics, December 2003 Vol. 17 (6), pp. 433–451.

[19] Muhammad Amjad Sohail et al" Effect of Turbulence Modeling on Aerodynamics characteristics of a conventional tailed finned missile configurations" CFP1070K-PRT, ISBN=11-4244-8101-9 Singapore 2010

[20] *Muhammad Yamin Younis., Muhammad Amjad Sohail, Tawfiqur Rahman, Zaka Muhammad, Saifur Rahman Bakaul"* Applications of AUSM+ Scheme on Subsonic, Supersonic and Hypersonic Flows Fields" Journal of World Academy Of Science, Engineering and Technology Issue 73 January 2011

[21] Wilcox DC. Turbulence modeling for CFD, 2nd ed.. LaCan˜ ada, CA: DCW Industries, 2002.

[22] Forsythe, J.R., Hoffmann, K.A., Cummings, R.M., Squires, K.D.., "Detached-Eddy Simulation with Compressibility Corrections Applied to a Supersonic Axisymmetric Base," *Journal of Fluids Engineering*, Vol. 124, No. 4, 2002, pp. 911-923.

[23] Morton, S.A., Forsythe, J.R., Mitchell, A.M., and Hajek, D., "Detached-Eddy Simulations and Reynolds-Averaged Navier-Stokes Simulations of Delta Wing Vortical Flowfields," *Journal of Fluids Engineering*, Vol. 124, No. 4, 2002, pp. 924-932.

[24] Squires, K.D., Forsythe, J.R., and Spalart, P.R., "Detached-Eddy Simulation of the Separated Flow Around a Forebody Cross-Section," Direct and Large Eddy Simulation IV, ERCOFTAC Series – Volume 8, B.J. Geurts, R. Friedrich and O. Metais, editors, Kluwar Academic Press, pp. 481-500, 2001.

[25] Forsythe, J.R., Squires, K.D., Wurtzler, K.E. and Spalart, P.R., "Detached-Eddy Simulation of Fighter Aircraft at High Alpha", AIAA 2002-0591, January 2002.

[26] Forsythe, J.R., Woodson, S.H., "Unsteady CFD Calculations of Abrupt Wing Stall Using Detached-Eddy Simulation", *AIAA 2003-0594*, Jan 2003

[27] Baldwin B, Lomax H. Thin-layer approximation and algebraic model for separated turbulent flows. AIAA Paper 78-257, January 1978.

[28] Hartwich PM, Hall RM. Navier–Stokes solutions for vortical flows over a tangent-ogive cylinder. AIAA J 1990; 28(7):1171–9

[29] Vatsa VN. Viscous flow solutions for slender bodies of revolution at incidence. Comput Fluids 1991;23(3):313–20

[30] Josyula E. Computational simulation improvements of supersonic high-angle-of-attack missile flows. J Spacecr Rockets 1999;36(1):59–66.
[31] Spalart PR, Allmaras SR. A one-equation turbulence model for aerodynamic flows. AIAA Paper 92-0439, January 1992
[32] Strelets M. Detached eddy simulation of massively separated flows. AIAA Paper 2001-0879, January 2001
[33] Forsythe JR, Hoffmann KA, Cummings RM, Squires KD. Detached-eddy simulation with compressibility corrections applied to a supersonic axisymmetric base flow. J Fluids Eng 2002;124(4):911–23.
[34] Squires KD, Forsythe JR, Spalart PR. Detached-eddy simulation of the separated flow around a forebody cross-section. In: Geurts BJ, Friedrich R, M! etais O, editors. Direct and large-eddy simulation IV. Dordrecht: Kluwer Academic Publishers, 2001. p. 481–500
[35] Travin A, Shur M, Strelets M, Spalart P. Detached-eddy simulations past a circular cylinder. Flow Turbulence Combust 2000;63(1):293–313
[36] TZONG-SHYNG LEU*, JENG-REN CHANG and CHUN-LIN KUO" EXPERIMENTAL INVESTIGATION OF SLENDERNESS EFFECT ON SIDE FORCE OF SLENDER BODY" Modern Physics Letters B, Vol. 24, No. 13 (2010) 1413−1416
[37] Philipe R. Spalart "Young's persons guide for detached eddy simulations Grid generations" NASA/CR-2001-211032
[38] Schiff LB, Degani D, Cummings RM. Computation of three dimensional turbulent vortical flows on bodies at high incidence. J Aircr 1991;28(10):689–99
[39] Thompson J, Matlin C, Gatlin B. Analysis and control of grid quality in computational simulation. Wright Laboratory TR-91-83, June 1992
[40] Mitchell A, Morton S, Forsythe J. Analysis of delta wing vortical substructures using detached-eddy simulation. AIAA Paper 2002-2968, June 2002.
[41] Morton SA, Forsythe JR, Mitchell AM, Hajek D. Detached-eddy simulations and Reynolds-averaged Navier–Stokes simulations of delta wing vortical flow-fields. J Fluids Eng 2002;124(4):924–32
[42] Forsythe JR, Squires KD, Wurtzler KE, Spalart PR. Detached-eddy simulation of fighter aircraft at high alpha, AIAA Paper 2002-0591, January 2002
[43] M. Shur, P. R. Spalart, M. Strelets, and A. Travin. Detached-Eddy Simulation of an Airfoil at High Angle of Attack. In *4th Int. Symposium on Eng. Turb. Modeling and Experiments*, Corsica, France, May 1999.
[44] Scott A. Morton" High Reynolds Number Detached-Eddy Simulations of Vortex Breakdown Over A 70 Degree Delta Wing"
[45] B. CARUELLEa, and F. DUCROSb" Detached-Eddy Simulations of Attached and Detached Boundary Layers" International Journal of Computational Fluid Dynamics, December 2003 Vol. 17 (6), pp. 433–451
[46] ANDREI TRAVIN, MICHAEL SHUR, MICHAEL STRELETS and PHILIPPE SPALART" Detached-Eddy Simulations Past a Circular Cylinder" *Flow, Turbulence and Combustion* 63: 293–313, 1999
[47] S. Venkateswaran,J. M.Weiss,andC. L.Merkle. Propulsion Related Flowfields Using the Preconditioned Navier-Stokes Equations. Technical Report AIAA-92-3437, AIAA/ASME/SAE/ASEE 28th Joint Propulsion Conference, Nashville, TN, July 1992
[48] T. Cebeci, and P. Bradshaw, *Momentum Transfer in Boundary Layers*, Hemisphere Publishing Corporation, New York, (1977)